ACS Photonics

Article

pubs.acs.org/journal/apchd5

Coevaporated Bisquaraine Inverted Solar Cells: Enhancement Due to Energy Transfer and Open Circuit Voltage Control

Tenghooi Goh,[†] Jing-Shun Huang,[†] Elizabeth A. Bielinski,[‡] Bennett A. Thompson,[‡] Stephanie Tomasulo,[§] Minjoo L. Lee,[§] Matthew Y. Sfeir,[∥] Nilay Hazari,[‡] and André D. Taylor*[,†]

Departments of [†]Chemical and Environmental Engineering, [‡]Chemistry, and [§]Electrical Engineering, Yale University, New Haven, Connecticut 06511, United States

[∥]Center for Functional Nanomaterials, Brookhaven National Laboratory, Upton, New York 11973, United States

Supporting Information

ABSTRACT: There is currently enormous interest in the development of small molecule organic solar cells (SMSC), as in principle, these systems offer advantages over both conventional Si photovoltaics and organic polymer solar cells. Here, we report Förster Resonance Energy Transfer (FRET) enhanced inverted SMSC fabricated by coevaporating two different squaraine donors, a symmetrical squaraine (SQ, 2,4-bis-4-[(*N*,*N*-diisobutylamino)-2,6-dihydroxyphenyl] squaraine), and an asymmetrical squaraine (ASSQ, 2,4-bis-[(*N*,*N*-diisobutylamino)-2,6-dihydroxyphenyl]-4-(4-diphenyliminio) squaraine). ASSQ absorbs blue light (λ_{max} 540 nm) and emits from 550 nm to the near-infrared region, which overlaps with SQ absorption (λ_{max} 690 nm). Therefore, by utilizing a thin film containing the two squaraine donors as the active layer in a SMSC, we can both broaden the photovoltaic absorption spectrum, and reduce recombination loss as a result of FRET. This strategy has resulted in SMSC with power conversion efficiencies (PCE) which are up to 46% greater than those obtained by using a single squaraine donor. Ultrafast time-resolved photoluminescence and transient absorption spectroscopy provide clear evidence of FRET between the small molecules, with a rapid energy transfer time of ∼1 ps. At optimal blending, which correlates to the highest PCE measured, the efficiency of energy transfer is as high as 85%. Furthermore, in the devices containing two different squaraine molecules, the open circuit voltage (V_{OC}) is proportional to the fraction of the two donors in the blend, allowing us to predict the V_{OC} as the ratio of the two donors is changed. SMSC with inverted structures also demonstrate long-term stability in ambient conditions compared to devices employing a conventional architecture.

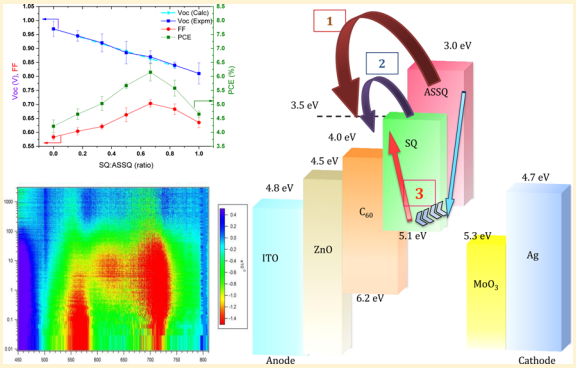

KEYWORDS: *small-molecule solar cells, Förster resonance energy transfer, open circuit voltage control, thermal coevaporation, photophysics*

Organic solar cells are widely regarded as attractive alternatives to traditional silicon solar cells.[1−3] The most well studied organic solar cells are those that contain conjugated polymers in the active layer, but in recent years, organic photovoltaics that contain small molecules as the photoactive material have received significant attention.[4] Organic photovoltaics with small molecules in the active layer share some of the benefits of organic polymer solar cells, as in principle they could also result in lightweight, flexible, low-cost, and vacuum- and solution-processable devices.[5] However, small molecules also offer several advantages[6] over polymers such as (i) they often have higher light absorption coefficients, (ii) in some cases they can be purified by sublimation or recrystallization as trace impurities can severely jeopardize solar cell performance,[7] (iii) thin films can be generated through vacuum deposition which leads to higher quality devices, and (iv) they have well-defined structures with distinct molecular weights, which leads to high repeatability and reliability in large scale synthesis without the problems associated with precise reproduction of chain length, polydispersity, and regioregularity. At this a stage a family of small molecules based on squaraine type dyes stand out as simple yet effective light harvesting dyes for photovoltaics[8] and also excel in various related applications such as photodetection,[9] optical data storage,[10] light emitting field effect transistors,[11] nonlinear spectroscopy,[12,13] biofluorescence imaging,[14] and photodynamic therapy.[15]

The blending of multiple photoactive materials to form a ternary solar cell is regarded as a simple and elegant strategy[16] to address two of the major limitations of organic solar cells; the relatively narrow absorption window and the lack of tunability of the open circuit voltage (V_{OC}). Unlike tandem

Received: August 1, 2014
Published: December 10, 2014

DOI: 10.1021/ph500282z
ACS Photonics 2015, 2, 86−95

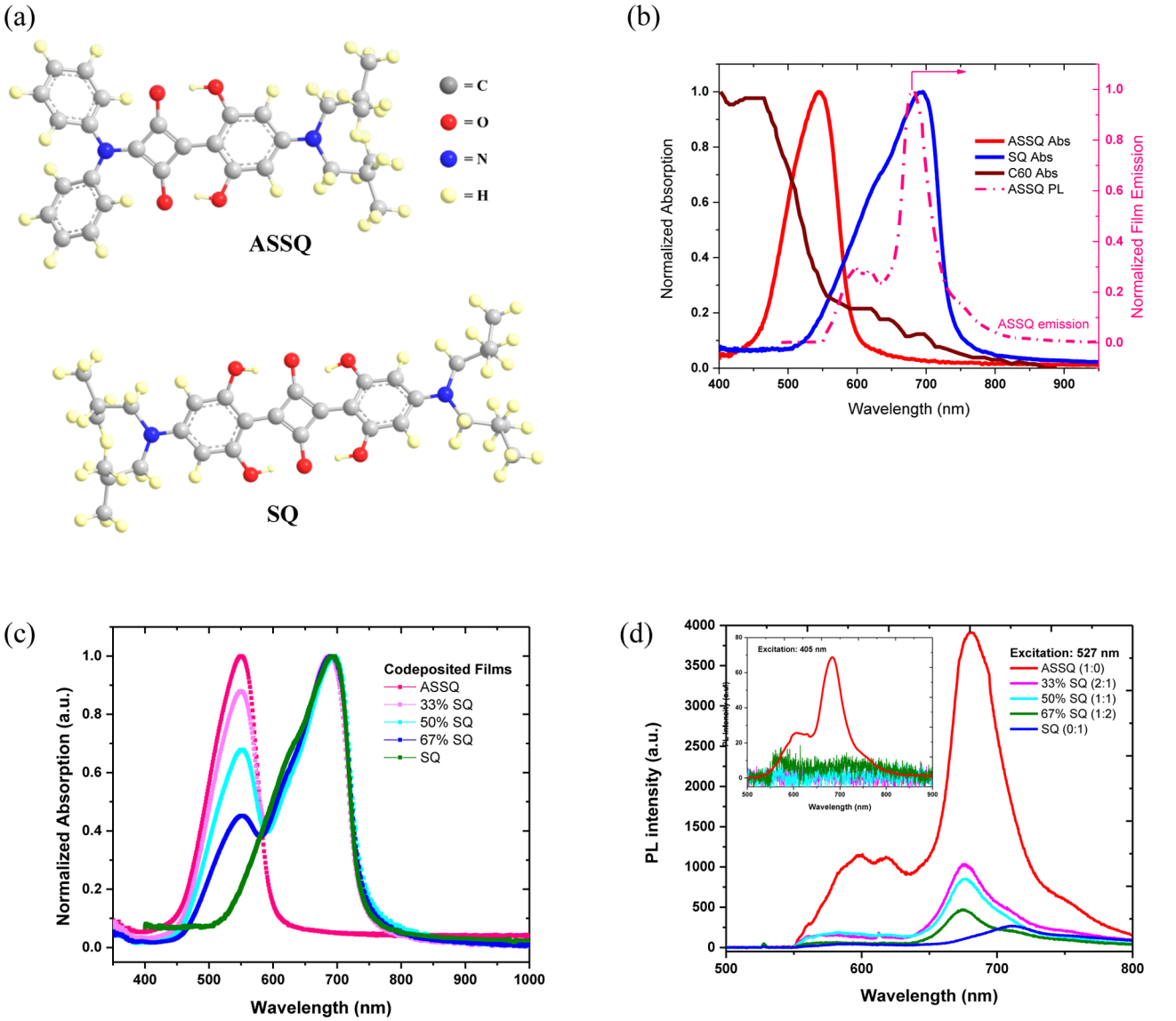

Figure 1. Optical properties of SQ and ASSQ. (a) Chemical structures of SQ and ASSQ. (b) Normalized absorption of thermally evaporated thin films of ASSQ (red), SQ (blue), and C_{60} (black) on the left axis; with the ASSQ emission (red dot) spectrum when excited at 500 nm on the right axis. (c) Absorption spectrum of the codeposited blended films with different ratios of ASSQ and SQ. (d) Steady state photoluminescence (PL) spectra of ASSQ and SQ blended films when excited at 527 and 405 nm (inset).

solar cells which broaden light harvesting by stacking multiple photoactive layers, a ternary solar cell is designed to achieve this goal by adding an infrared (IR) sensitizer into the host matrix.[17−19] This architecture bypasses technical challenges associated with the reliability and reproducibility of multijunction solar cells. It is currently proposed that there are three main mechanisms that explain the improvement observed in many ternary solar cells: (i) charge transfer, (ii) energy transfer, and (iii) parallel linkage.[20] We suggest that, with careful design, ternary solar cells can be pushed toward even higher efficiencies by combining the benefits of these mechanisms. In fact, optimization of these factors could eventually result in a single-junction organic photovoltaic which surpasses the proposed efficiency limit of 17%.[21]

Recently, it has been demonstrated that Förster resonance energy transfer (FRET) can be used to improve the efficiency of both dye sensitized solar cells and organic polymer cells. For example, studies using a variety of different dye-sensitized solar cells have shown that FRET can lead to amplified charge injection,[22] an increase in the stability of the electrolyte,[23] optimized dye loading,[24] an 89% boost in photocurrent,[25] and most impressively a doubling in the power conversion efficiency (PCE).[26] Furthermore, in the only well characterized report of FRET in organic polymer solar cells, our group demonstrated that FRET improved the PCE of ternary blend polymer solar cells by up to 38%, by both increasing the spectral range of the photons captured and reducing energy loss through exciton recombination.[27] Very recently, a remarkable 8.4% PCE was also achieved by exploiting FRET enhancement on multilayer cascade devices.[28] While many reports on ternary solar cells have discussed the effects of Voc modification[29,30] and morphology enhancement by annealing[31] and mixing,[32,33] we show that improvement can also be achieved by photophysical methods in mixed donor devices. Specifically, in this work, we devise and implement a strategy to employ FRET in ternary small molecule organic solar cells. By concurrently thermally

DOI: 10.1021/ph500282z
ACS Photonics 2015, 2, 86−95

depositing two squaraine-based dyes, with complementary absorption and emission, we have fabricated highly efficient and durable inverted small molecule organic solar cells. FRET enhancement, which has been confirmed using ultrafast transient spectroscopy, results in ternary small molecule organic solar cells with PCEs of over 6% and fill factors (FF) above 70%. This represents an improvement of up to 46% compared to small molecule organic solar cells, which only contain one squaraine based dye. Our work is distinct from the pioneering research of Forrest and other groups[34,35] because it focuses on photophysical effects in ternary solar cells containing multiple squaraines rather than on the device morphology.

RESULTS AND DISCUSSION

Electronic Properties of Donor Materials and the Optical Origin of FRET. The molecular structures of assymetrical squaraine (ASSQ) and symmetrical squaraine (SQ) are illustrated in Figure 1a. These molecules contain an electron-withdrawing four-membered-ring derived from squaric acid, bonded to two electron donating moieties to form donor−acceptor−donor structures. In both cases, the planar and extended π-framework of these dyes results in high absorption coefficients ($\geq 10^5$ cm^{-1}).[36] In addition, the bulky *N*,*N*-diisobutyl side groups provide stability for sublimation,[37] while the *N*,*N*-diphenyl substituent in ASSQ promotes charge transport[38] and results in longer exciton diffusion lengths.[34] Thermogravimetric analysis (TGA) further reveals that both dyes have relatively high decomposition temperatures of around 300 °C (Supporting Information, Figure S5).

Figure 1b shows the normalized UV−vis absorption spectra of thermally evaporated ASSQ, SQ, and C_{60} thin films, along with the emission spectrum of an ASSQ thin film. The peak absorption band of ASSQ (λ_{max} 543 nm) complements SQ's absorption (λ_{max} 695 nm) in the near-infrared (NIR) region. Together, the ASSQ-SQ blends form films with extended photoresponse range, spanning over the entire visible spectrum, as depicted in Figure 1c, where the absorption spectra of thin films containing different ratios of ASSQ and SQ (normalized to the SQ peak intensity at 695 nm) are shown.

In order for FRET to occur, it is necessary to have spectral overlap between the donor emission and acceptor absorption profile, as depicted for ASSQ and SQ in the inset of Figure 1b and Supporting Information, Figure S2. In fact, the efficiency of energy transfer is closely linked to the degree of overlap between the absorption and emission.[24] As illustrated by the dotted line in Figure 1b, the photoluminescence (PL) emission of ASSQ peaks at 680 nm and matches the SQ absorption window almost exactly. The shoulder at 550−640 nm of ASSQ PL may be caused by two-photon absorption, which has been reported in other types of squaraines.[39] The Forster radius, R_0, refers to the distance between the donor and acceptor at which energy transfer efficiency is 50%. In this case, the R_0 between ASSQ and SQ is estimated to be 4.3 nm using conservative assumptions (Supporting Information, Figure S2), based on diluted squaraines dissolved in chloroform. This number is comparable to that reported for FRET pairs in other systems utilized for solar cells to date.[24−26,40]

When thin films containing both SQ and ASSQ were excited by a steady laser beam at 527 nm (which should selectively excite ASSQ and not SQ), the PL intensity of ASSQ was quenched. The quenching efficiency (eq 1) can be used to quantify energy transfer from the relative peak intensity (I) in Figure 1d, where a higher numerical value indicates greater energy transfer.

$$\Phi_q = \frac{I_{ASSQ} - I}{I_{ASSQ}} \times 100\% \quad (1)$$

The values of Φ_q for blended films with 33, 50, and 67% SQ are 78, 82, and 92%, respectively. When excited with a light source at 405 nm, ASSQ retains the same PL profile with a much lower intensity, due to low absorption at this wavelength. These excitons are quickly quenched, even with small amounts of SQ, which may indicate that the binary films are homogeneously blended and that effective energy transfer can occur even if the quencher is only present in a small amount. Overall, the optical data strongly suggest that ASSQ and SQ are excellent candidates for forming an effective FRET pair in a photovoltaic device.

Analyzing the energy levels of the components in an organic solar cell can help provide insight on charge transport, exciton dissociation, and the probability of FRET.[40] When an incoming photon is absorbed by a chromophore, a geminate exciton can be generated, which will eventually recombine back to the ground state either by radiationless relaxation or photon emission. This will lower the efficiency of the device. When energy conservation, spatial, and optical requirements are met, FRET can stimulate an oscillating electric field to sensitize the acceptor. The geminate recombination loss can be partially "recovered" by transferring energy for exciton generation in the FRET acceptor molecule (Figure 2a). This process takes place without light absorption by the FRET acceptor, and leads to a reduction in the donor's fluorescence intensity and excited state lifetime.

Figure 3a illustrates a schematic of the architecture of our inverted solar cells. The highest occupied molecular orbital (HOMO) and lowest unoccupied molecular orbital (LUMO) energy levels of each component in the inverted solar cells are plotted in Figure 2b, based on the values reported in the literature.[34,41,42] The cascade band edge alignment of the squaraine dyes and C_{60} establishes a suitable energy offset for exciton dissociation and offers two pathways for charge transport. In addition, ASSQ introduces a third route by funneling energy to SQ via FRET. Hence, this picture suggests that photocurrent enhancement is possible, compared to conventional single donor−acceptor bilayer solar cells.

Photovoltaic Performance. To study ternary blend small molecule organic solar cells, we fixed the thickness of the blend-donor layer to 30 nm and fabricated a series of devices with varying amounts of ASSQ and SQ. The $J-V$ characteristics of ASSQ-SQ/C_{60} organic solar cells at 1 sun illumination are shown in Figure 3b, with the average photovoltaic parameters over at least 16 devices are summarized in Table 1. The control devices containing only ASSQ or SQ attained PCEs of 4.2% ± 0.2 and 4.7% ± 0.1, respectively. Our results clearly indicate that ternary solar cells perform much better than devices containing only a single dye. The highest efficiency of a ternary solar cell is 6.2% ± 0.3, which was achieved using a ratio of ASSQ to SQ of 1:2 (or 67% SQ). This blending ratio gives the highest short circuit current (J_{SC} = 10.1 ± 0.2 mAcm^{-2}) and FF (70% ± 0.1). Overall, the optimal mixed donor cell gives an improvement in efficiency of 33% compared to a neat SQ solar cell or 46% if benchmarked to a neat ASSQ device.

Although the significant improvement in J_{SC} in our ternary small molecule organic solar cells can be partially explained by

DOI: 10.1021/ph500282z
ACS Photonics 2015, 2, 86−95

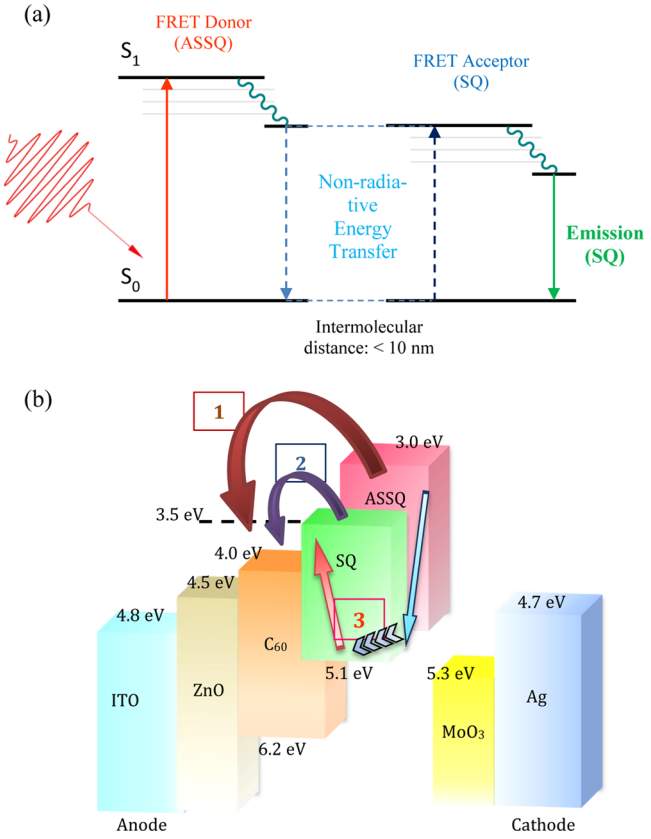

Figure 2. Construction and energy level diagram of the blend donor device. (a) Schematic illustrating a simple FRET mechanism (note that the proper energy level alignment between donor and acceptor is essential for FRET to occur). (b) Theoretical HOMO and LUMO of the components of the ternary blend solar cell where three pathways of charge and energy transfer are highlighted. For simplicity, the mixed SQ-ASSQ film is depicted as an individual layer in the schematic representation.

the broader absorption range for blended films, we have demonstrated in ternary organic polymer solar cells that this is not the only factor that can be responsible for an increase in J_{SC}.[27] To further understand the effects of the ternary small molecule blend on the increase in photocurrent, external quantum efficiency (EQE) measurements were performed (Figure 3b). In agreement with the absorption data in Figure 1, the range of spectral absorption is significantly larger in mixed donor devices. The EQE measurements show that there are four distinct peaks. The highest energy peak at 347 nm corresponds to C_{60} absorption. The next highest energy peaks at approximately 455 and 555 nm are attributed to ASSQ and C_{60} absorption (refer to the neat ASSQ curve in red), while SQ is responsible for the near-infrared (NIR) peak at 700 nm. There is no change in the quantum efficiency of the near UV peak (347 nm) as the ASSQ to SQ ratio is changed, which is consistent with the C_{60} film thickness remaining constant in all of the devices. However, the peaks at 455 and 555 nm, in particular, the peak at 455 nm, display interesting photocurrent enhancement effects, which are only present in the blended films. The specific EQE at 455 nm of neat SQ and ASSQ devices are only 40 and 48%, respectively. However, as SQ is coblended with ASSQ, the resultant device EQE at 455 nm increases from 51% to 53% to 56% at SQ concentrations of 33%, 50%, and 67% in the coblend. While it may seem counterintuitive that more SQ leads to higher photocurrent in this region of the spectrum, we believe that FRET is responsible for the surge in EQE (vide infra). In a neat ASSQ film, a significant portion of the photoexcited ASSQ loses energy through recombination and does not result in photocurrent. When nearby SQ molecules are present, less recombination occurs, because some of the photoexcited ASSQ nonradiatively transfers energy to SQ, which eventually translates to higher photocurrent, despite lower light absorption. Finally, the EQE of the NIR peak strongly correlates to the proportion of SQ in the devices, which is a direct consequence of only SQ absorbing photons in this region.

In the design of ternary blend solar cells the impact of the two active materials on the V_{OC} is an important consideration. The V_{OC} of most organic solar cells is known to be related to the offset between the energy levels of the acceptor's LUMO and the donor's HOMO. Equation 2 predicts a V_{OC} of ~1 V for a neat ASSQ device and 0.8 V for a neat SQ device, when C_{60} is used as the acceptor, showing good agreement with our experimental data and results reported by Forrest and co-workers.[34,43]

$$V_{OC} \approx (1/e)(|E^{donor}{}_{HOMO}| - |E^{C_{60}}{}_{LUMO}|) - 0.3\ V \quad (2)$$

Figure 3d highlights the changes in V_{OC}, FF, and J_{SC} as the ASSQ to SQ ratio is varied. Equation 2, despite demonstrating good agreement with the empirical V_{OC} for neat films, is not applicable in predicting the V_{OC} of blended films. However, our results indicate that in blended devices there is a linear relationship between V_{OC} and the donor fraction, using the relationship shown in eq 3.

$$V_{OC} = \rho(V_{SQ-C_{60}}) + (1 - \rho)(E_{DA-ASSQ}) \quad (3)$$

where ρ is the fraction of SQ deposited and $V_{SQ\text{-}C60}$ and $V_{ASSQ\text{-}C60}$ denote the open circuit voltage of neat SQ/C_{60} and ASSQ/C_{60} devices, respectively.

The experimental V_{OC} values are compared to those calculated using eq 3 in Table 2. There is excellent agreement, which suggests that the V_{OC} can be controlled by tuning the relative donor concentrations. Previously, some other groups have also observed a linear relationship between V_{OC} and the relative concentration of the donor materials in ternary solar cells, suggesting that this may be a general phenomenon.[30,43,44]

At this stage, the nature of the recombination processes in small molecule organic solar cells have not been fully identified.[45] We attempted to relate recombination to device performance by estimating the ideality factor, n, from the modified diode formula, eq 4, described by Giebink et al.[46,47]

$$J = J_S\left[\exp\left(\frac{q(V - JR_s)}{nk_bT}\right) - \left(\frac{k_{ppd}}{k_{ppd,eq}}\right)\right] + \frac{V - JR_s}{R_{sh}} \quad (4)$$

where J_S is the reverse saturation current density; q is the electron charge; R_s is the series resistance; R_{sh} is the shunt resistance; k_b refers to Boltzmann constant; T is temperature in Kelvin; and $k_{ppd}/k_{ppd,eq}$ is the ratio of polaron pair dissociation rate to its equilibrium value, which is assumed to be 1 for simplicity.

We show that the FF and J_{SC} increase as the percentage of SQ in the devices increases (Figure 3d), until the optimal blending ratio is reached. At this point, both the FF and J_{SC} decrease as the percentage of SQ increases. The decline in FF

DOI: 10.1021/ph500282z
ACS Photonics 2015, 2, 86−95

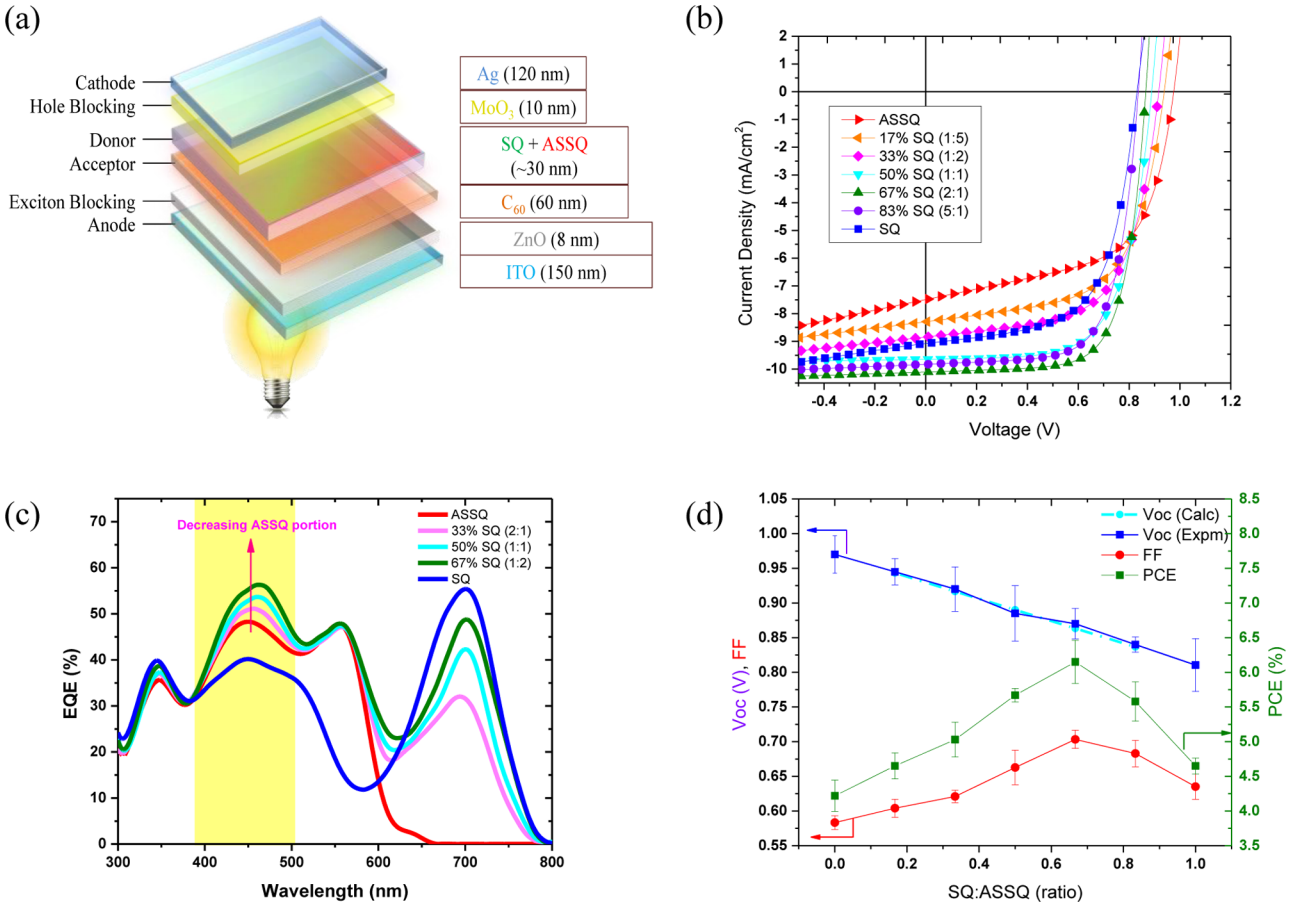

Figure 3. Solar cell performance: impact of blending ratio. (a) Cross section of the architecture and thickness of each layer of the inverted small molecule solar cells. (b) The $J-V$ curves of photovoltaic devices with different ASSQ to SQ ratios under 100 mW cm^{-2} AM 1.5G irradiation. (c) External quantum efficiency (EQE) vs wavelength of the co-donor devices. (d) Plots of V_{OC}, FF, PCE vs the blending fraction of SQ. The experimental V_{OC} (blue) agrees with the calculated V_{OC} (cyan).

Table 1. Summary of the Average Photovoltaic Parameters and Efficiencies of Solar Cells with Different Ratios of SQ and ASSQ, Measured under AM1.5G Solar Illumination (100 mW cm^{-2})

ASSQ/SQ ratio	SQ % (%)	V_{OC} (V)	J_{SC} (mA/cm^2)	FF (%)	n	R_{Sh} (Ω/cm^2)	R_S (Ω/cm^2)	PCE (%)
1:0	0	0.97	7.46	58.3	1.76	76.9	2.03	4.22
5:1	16.7	0.95	8.10	60.4	1.86	86.3	1.69	4.65
2:1	33.3	0.92	8.81	62.1	1.89	99.0	1.59	5.03
1:1	50.0	0.89	9.62	66.3	1.65	681.0	1.43	5.67
1:2	66.7	0.87	10.05	70.3	1.72	331.7	1.12	6.15
1:5	83.3	0.84	9.73	68.4	1.93	259.2	1.17	5.58
0:1	100	0.81	9.05	63.5	1.84	326.1	1.68	4.65

Table 2. Comparison of the Calculated Open Circuit Voltage Based on a Linear Combination of the Fraction of Each Donor vs the Experimental Values

fraction ρ(SQ)	calcd V_{OC} (V)	mean experimental V_{OC} (V)
1		0.811 ± 0.04
5/6	0.84	0.840 ± 0.01
2/3	0.86	0.872 ± 0.02
1/2	0.89	0.885 ± 0.04
1/3	0.92	0.921 ± 0.03
1/6	0.94	0.945 ± 0.02
0		0.972 ± 0.03

and J_{SC} is accompanied by an increase in the ideality factor, and values close to 2 are calculated at higher SQ concentration. This implies that bimolecular recombination becomes more prevalent at higher SQ concentration, a result of a more prominent trapping mechanism, which is consistent with work by Kang et al. on other ternary blends.[48] Furthermore, the trends in series resistance R_s (estimated from the inverse slope of V_{OC} in the individual $J-V$ curves) and shunt resistance R_{sh}, signify a better FF for the blended films. The R_s and R_{sh} terms originate from the concept of an equivalent diode circuit with R_s being related to the resistive loss of the maximal photocurrent, while R_{sh} quantifies the current leakage from pinholes and traps.[49] The control ASSQ device reports the highest R_s at 2.0 Ω·cm^2 and the lowest R_{sh} at 76.9 Ω·cm^2. Incorporation of SQ generally lowers R_s, while R_{sh} increases at first and then decreases. The optimal cells with 67% SQ strike a balance between the two parameters, suggesting that active

DOI: 10.1021/ph500282z
ACS Photonics 2015, 2, 86−95

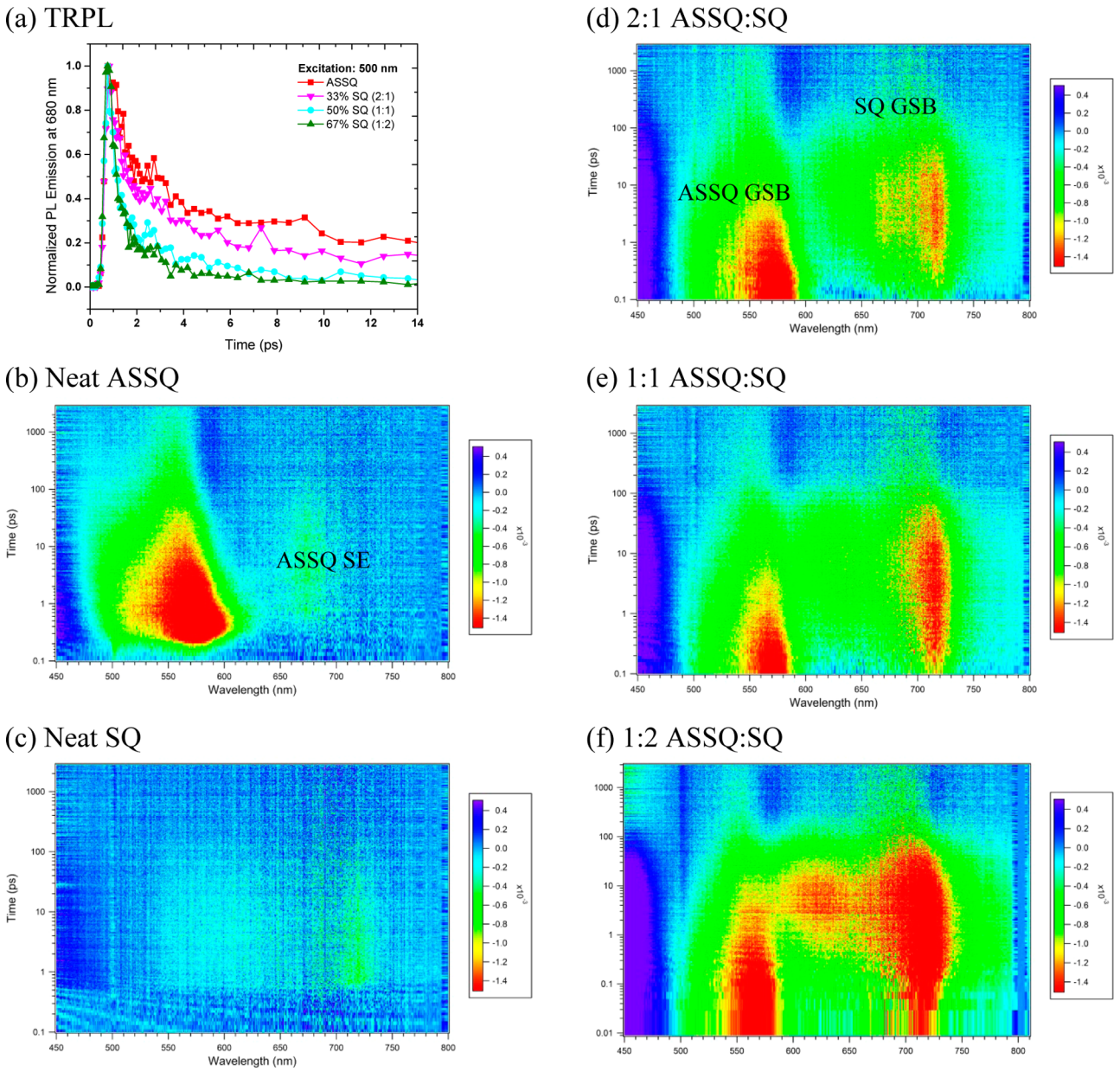

Figure 4. Photophysics study. (a) Time-resolved photoluminescence decay traces of a neat ASSQ film and ASSQ/SQ blended films. (b–f) Transient absorption spectroscopy of neat ASSQ (b), SQ (c), and blended films mixed in ASSQ/SQ ratios of 2:1 (d), 1:1 (e), and 1:2 (f). The pumping wavelength was set at 500 nm, with a fluence of 16 μJ cm^{-2}. The spectra in (d), (e), and (f) are fixed at the same color contour scale for ease of comparison.

layers with more SQ lead to interfaces with less series resistance, while maintaining a satisfactory rectification effect. The reason for reduced R_s caused by SQ is yet unclear, but it could be associated to higher packing density in SQ.[50] Studies have shown that denser packing could improve carrier mobility and thus translate to higher FF.[51]

The increase in the FF and PCE at the 1:2 ASSQ/SQ ratio can also be correlated with an increase in crystallinity as shown by the grazing-incident wide-angle X-ray scattering (GIWAXS) results (Supporting Information, Figure S7a). We notice that film crystallinity was enhanced at this blending ratio, especially at the out-of-plane direction, which associates to better charge transport, and thus increased fill factor. Out-of-plane linecut (Supporting Information, Figure S7b) also shows that most of the squaraine films demonstrate π–π stacking distance of ∼2.8 and 3.2 Å, while a 1:2 (ASSQ/SQ) blend exhibits strong scattering peaks at 4.4 and 6.8 Å, indicating cocrystallinity of ASSQ and SQ at this ratio. The reason why the optimal blending ratio case promotes crystallinity is still under investigation. Molecular simulation and in-depth morphological studies will be conducted in the future.

A simple durability study was performed by comparing the performance of our inverted solar cells to a conventional solar cell with a 2:1 SQ to ASSQ ratio by exposing them to ambient air. The initial PCE of conventional ITO/PEDOT:PSS (3000 rpm, Clevios)/SQ-ASSQ/C_{60}/PTCBI/Al solar cells straight after device fabrication was 5.7%, with a V_{OC} of 0.91 V, J_{SC} of 9.8 mA/cm^2, and FF of 64.2%. The efficiencies of conventional and inverted solar cells were measured for the next 16 days and normalized to results obtained on day zero (Supporting

DOI: 10.1021/ph500282z
ACS Photonics 2015, 2, 86–95

Information, Figure S1). During the study, the cells were stored in air. Inverted solar cells demonstrated significantly better stability after 2 weeks, maintaining ∼74% of initial efficiency, as opposed to conventional devices, which only gave ∼7% of initial efficiency. This demonstrates that utilizing both a sol−gel derived ZnO buffer layer and a high work-function anode (Ag) extends device lifetime, as has been observed elsewhere.[42,52,53]

Photophysics and Photodynamics. Ultrafast time-resolved photoluminescence (TRPL) and transient absorption (TA) measurements were conducted to assist in understanding energy transfer between ASSQ and SQ. These studies were performed by fixing the pumping pulse at 500 nm to selectively excite ASSQ, but not SQ, and emission at 680 nm is detected for TRPL experiment, while laser fluence was limited below 20 uW to reduce the perturbation due to exciton−exciton annihilation.[54] The fluorescence decay of neat ASSQ and blended films, shown in Figure 4a, was fitted with a three-component-exponential function, and the mean lifetime was calculated by weighing the amplitude of each component, a_i. The energy transfer efficiency, ETE, was further quantified using eq 6.

$$\langle \tau \rangle = \frac{\sum_i^n a_i \tau_i^2}{\sum_i^n a_i \tau_i} \tag{5}$$

$$\mathrm{ETE} = 1 - \frac{\langle \tau_{\mathrm{blend}} \rangle}{\langle \tau_{\mathrm{ASSQ}} \rangle} \tag{6}$$

The mean time constant for neat ASSQ is 58.9 ps based on 3 exponential τ fitting from the decay profile measured by TRPL. When the SQ concentration is increased to 33%, 50%, and 67% (blending ratios of 2:1, 1:1, and 1:2), the time constant diminishes average exciton lifetime to 23.6, 19.9, and 9.0 ps, which translates to ETEs of 60%, 66%, and 85%, respectively. The ETE values are comparable to those observed in DSSCs,[24,55] and this trend suggests that there is efficient energy transfer at the optimal blending ratio, following the trend of photovoltaics performance at different blending ratios.

While TRPL probes the dynamics of ASSQ (donor) exciton only, the time- and spectra-resolved TA contour plots (Figure 4b−f) reveal a greater extent of information for excited and decayed species for neat ASSQ, SQ, and the intermediate blends. All of these 2D spectra share a common color contour to assist in the analysis. The data from neat ASSQ and SQ films are used as the baselines for comparison. In Figure 4b, the strong negative signal from 500 to 610 nm clearly corresponds to the ground state bleaching (GSB) of ASSQ, and the spontaneous emission (SE) at 660−690 nm is rather weak compared to the bleaching intensity. The SQ film produces only a very weak and narrow emission signal between 710 and 730 nm (Figure 4c). In contrast to the neat films, all of the blended films exhibit two strong features: (i) GSB of ASSQ; and (ii) GSB of SQ in the NIR region, which we have verified previously.[27] As the percentage of SQ is increased, the intensity of the GSB of ASSQ is reduced, while the GSB of SQ grows stronger. Given that SQ absorbs minimally at 500 nm, the presence of a GSB for SQ confirms FRET, where the excitation energy is channeled from the photoexcited ASSQ and results in SQ emission. Consistent with our previous observations, this trend implies that FRET is most prominent at the optimal ratio (ASSQ/SQ = 1:2).

In order to estimate the energy transfer time, the raw transient absorption data in Figure 4 was deconvoluted using global analysis methods.[35,56] Reconstruction of the decay associated spectra (DAS, which assumes parallel decay back to the ground state) and the evolution associated spectra (EAS, sequential decay of species) is accomplished using a sum of three first order decay processes. While the extracted rate constants agree in both models, the sequential treatment allows for a more direct physical visualization of the associated transient spectra associated with each distinct electronic species, that is, that species 3 (black, ultrafast energy transfer event) decays to form species 2 (red, concurrent ASSQ photobleaching and SQ stimulated emission), ensued by a long-lived species 1 (blue), before relaxation to ground states (Supporting Information, Figure S3). Moreover, this model allows us to visualize the population trajectory over time (Supporting Information, Figure S4). The recovered energy transfer rate constants for ASSQ/SQ blended films are 1.6 ps for the 2:1 ASSQ/SQ blend, 1.4 ps for 1:1, and 1 ps for 1:2. The rapid rate of energy transfer (∼1 ps) indicates that FRET occurs sufficiently quickly to compete with other photophysics processes such as recombination. In addition, the small sensitivity of measured rate constant as a function of SQ incorporation reaffirms high energy transfer efficiency between ASSQ and SQ and also implies the presence of large and comparable amount of ASSQ/SQ interfaces at any blend ratio.

CONCLUSIONS

In summary, we have developed a simple yet effective method to greatly improve the performance of small-molecule-based photovoltaics. Our results indicate that ternary blend solar cells containing two thermally deposited squaraine based dyes generally perform better than devices consisting of only one squaraine dye, with improvements of up to 46% observed, due to the increase in photocurrent (or J_{SC}). The increase in J_{SC} is caused both by the broader absorption spectrum of the blended devices and an enhancement through FRET, which limits recombination. Interestingly, in the coblended devices there is a linear dependency between V_{OC} and the amount of a donor material in the active layer, which suggests that the photoactive donors could structure themselves in a parallel- fashion.[57] It is also noteworthy that fabricating small molecule solar cells using an inverted architecture results in photovoltaics with increased stability compared to conventional devices. Furthermore, we believe that there are still several factors that can be optimized to improve the already high efficiency of our devices, such as (i) improving control of morphology by annealing,[32] (ii) increasing energy harvesting by replacing C_{60} with C_{70}[58] or a bis-indene functionalized fullerene (ICBA),[16] and (iii) enhancing the current collection by using a better charge injection layer.[59] Overall, this study shows that careful material selection and molecule design are required to strike a balance between photocurrent and photovoltage generation in organic solar cells.

METHODS

Synthesis, Purification, and Codeposition of SQ and ASSQ. Squaraine (SQ) was synthesized and purified using a literature procedure.[37] The synthesis of the asymmetrical squaraine, ASSQ, was based on a literature procedure but was modified and optimized as part of this work.[38] Details of the new synthesis are included in the Supporting Information. Squaraine dyes were stored inside a nitrogen-filled glovebox and further purified using a gradient sublimation unit integrated

DOI: 10.1021/ph500282z
ACS Photonics 2015, 2, 86−95

in the glovebox at 10^{-7} mbar. Sublimed squaraines were transferred into a ÅMOD chamber from Angstrom Engineering and deposited from multiple Luxel Radak thermal evaporators, with the heating temperatures controlled to be less than 180 °C for SQ and 155 °C for ASSQ.

Device Fabrication. ITO-coated thin glasses with a sheet resistance of ∼15 Ω/sq were purchased from Bayview Optics and patterned in-house with HCl, followed by wet-cleaning with deionized water, trichloroethylene, acetone, and isopropanol. The sol−gel method[42,53] was modified to deposit approximately 8 nm of ZnO by spin-coating at 3000 rpm, and the ensemble was baked at 250 °C for 10 min in the furnace with continuous air-flow (filtered). Sublimated-grade C_{60} 60 nm was then evaporated on the ZnO-coated ITO substrates at ∼1 Å/s, and the SQ and ASSQ blends were subsequently codeposited in the same chamber. The substrates were then transferred to another chamber for deposition of 10 nm MoO_3 and 120 nm Ag at a pressure of $\sim 10^{-7}$ Torr with shadow masks. Thicknesses of the evaporated films were estimated with built-in quartz crystal balance in the deposition chambers.

PCE and EQE Characterization. After fabrication, devices were illuminated at 100 mW cm^{-2} from a 150 W solar simulator with AM 1.5G filters (PV Measurements) inside our integrated N_2-filled glovebox without passivation. The active area of a standard single device irradiated by the light was defined as 5 mm^2 by using a shadow mask, to minimize cross-talking and overestimation of photocurrent. Current density−voltage (J−V) curves were measured with a Keithley 2400 source measurement unit. The device parameters are averages from the measurement of at least five individual devices. The absorption spectra of dried films and solutions were obtained using a Varian Cary 3E UV−vis spectrophotometer. The EQE measurements were performed in air using a PV Measurements QEX7 system.

Time-Resolved PL and Transient Absorption (TA) Measurements. Broadband TA spectra were obtained using an amplified Ti:sapphire laser system and optical parametric amplifier (OPA). Briefly, ∼20 nm of thermal evaporated neat SQ, ASSQ, and blended films (Spectra-Physics) were resonantly excited with ∼100 fs laser pulses generated by the OPA at a repetition rate of 80 MHz. Time-resolved absorption spectra were obtained using a femtosecond broadband supercontinuum probe pulse that was overlapped in time and space with the femtosecond pump pulse. The supercontinuum was produced by focusing a small portion of the amplified laser fundamental into a sapphire plate. Multiwavelength transient spectra were recorded using dual spectrometers (signal and reference) equipped with fast Si array detectors. In all experiments, the fluence value was fixed at 16 μJ cm^{-2} after determining the beam spot size. Chirping due to dispersion in the white probe beam was corrected before the data analysis.

Thermal Stability Measurement. TGA measurements were conducted with Q50 unit from TA Instruments. ∼ 5 mg of each squaraine was loaded and purged with N_2 for 30 min in the furnace before the actual test. The heating process was carried out in N_2 gas where the ramp rate was set at 5 °C/min. Decomposition temperature is determined by the peak of first derivative of the weight loss curve.

Grazing-Incident X-ray Scattering (GIXS). X-ray scattering experiments were performed at the X9 undulator-based beamline at the National Synchrotron Light Source. An incident X-ray beam of energy 13.5 keV (wavelength = 0.0918 nm) was collimated using a two-slit system and focused to a beam 100 μm wide by 60 μm tall at the sample position using a Kirkpatrick-Biaz mirror system. Samples were spin-coated on precleaned silicon wafers and mounted on a translation stack under vacuum ∼40 Pa. Grazing-incidence experiments were performed over a range of incidence angles (7−15 theta), both below and above the film-vacuum critical angle. Two-dimensional scattering images were measured in both the small-angle (GISAXS) and wide-angle (GIWAXS) using two charged-coupled device (CCD) detectors. The WAXS detector was positioned at 270 mm from the sample. Data conversion to q-space was accomplished using Silver Behenate powder as a standard.

■ ASSOCIATED CONTENT

Supporting Information

For device durability performance, thermal stability, photodynamics, GIWAXS data, and global fitting spectrum and details on improved ASSQ synthesis. This material is available free of charge via the Internet at http://pubs.acs.org.

■ AUTHOR INFORMATION

Corresponding Author

*E-mail:andre.taylor@yale.edu

Notes

The authors declare no competing financial interest.

■ ACKNOWLEDGMENTS

The authors gratefully acknowledge the National Science Foundation (DMR-1410171) and the Yale Climate and Energy Institute (YCEI) for partial support of this work. A.D.T. also acknowledges support from the NSF-CAREER award (CBET-0954985). The authors appreciate the help of Dr. Kevin Yager with the GIWAXS experiments. This research was carried out in part at the Center for Functional Nanomaterials, Brookhaven National Laboratory, which is supported by the U.S. Department of Energy, Office of Basic Energy Sciences, under Contract No. DE-AC02-98CH10886. Facilities use was supported by YINQE and NSF MRSEC DMR 1119826 (CRISP).

■ REFERENCES

(1) Heeger, A. J. 25th Anniversary Article: Bulk Heterojunction Solar Cells: Understanding the Mechanism of Operation. *Adv. Mater.* **2014**, *26*, 10−28.

(2) Darling, S. B.; You, F. The Case for Organic Photovoltaics. *RSC Adv.* **2013**, *3*, 17633−17648.

(3) Dou, L.; You, J.; Hong, Z.; Xu, Z.; Li, G.; Street, R. A.; Yang, Y. 25th Anniversary Article: A Decade of Organic/Polymeric Photovoltaic Research. *Adv. Mater.* **2013**, *25*, 6642−6671.

(4) Huang, Q.; Li, H. Recent Progress of Bulk Heterojunction Solar Cells Based on Small-Molecular Donors. *Chin. Sci. Bull.* **2013**, *58*, 2677−2685.

(5) Mishra, A.; Bäuerle, P. Small Molecule Organic Semiconductors on the Move: Promises for Future Solar Energy Technology. *Angew. Chem., Int. Ed.* **2012**, *51*, 2020−2067.

(6) Seifter, J.; Sun, Y.; Heeger, A. J. Transient Photocurrent Response of Small-Molecule Bulk Heterojunction Solar Cells. *Adv. Mater.* **2014**, *26*, 2486−2493.

(7) Nikiforov, M. P.; Lai, B.; Chen, W.; Chen, S.; Schaller, R. D.; Strzalka, J.; Maser, J.; Darling, S. B. Detection and Role of Trace Impurities in High-Performance Organic Solar Cells. *Energy Environ. Sci.* **2013**, *6*, 1513−1520.

DOI: 10.1021/ph500282z
ACS Photonics 2015, 2, 86−95

(8) Chen, G.; Sasabe, H.; Wang, Z.; Wang, X.-F.; Hong, Z.; Yang, Y.; Kido, J. Co-Evaporated Bulk Heterojunction Solar Cells with >6.0% Efficiency. *Adv. Mater.* **2012**, *24*, 2768−2773.
(9) Zhang, Y.; Deng, W.; Zhang, X.; Zhang, X.; Zhang, X.; Xing, Y.; Jie, J. In Situ Integration of Squaraine-Nanowire-Array-Based Schottky-Type Photodetectors with Enhanced Switching Performance. *ACS Appl. Mater. Interfaces* **2013**, *5*, 12288−12294.
(10) Emmelius, M.; Pawlowski, G.; Vollmann, H. W. Materials for Optical Data Storage. *Angew. Chem., Int. Ed.* **1989**, *28*, 1445−1471.
(11) Qu, J.; Zhang, J.; Grimsdale, A. C.; Müllen, K.; Jaiser, F.; Yang, X.; Neher, D. Dendronized Perylene Diimide Emitters: Synthesis, Luminescence, and Electron and Energy Transfer Studies. *Macromolecules* **2004**, *37*, 8297−8306.
(12) Webster, S.; Odom, S. A.; Padilha, L. A.; Przhonska, O. V.; Peceli, D.; Hu, H.; Nootz, G.; Kachkovski, A. D.; Matichak, J.; Barlow, S.; Anderson, H. L.; Marder, S. R.; Hagan, D. J.; Van Stryland, E. W. Linear and Nonlinear Spectroscopy of a Porphyrin−Squaraine−Porphyrin Conjugated System. *J. Phys. Chem. B* **2009**, *113*, 14854−14867.
(13) Makowski, B. T.; Valle, B.; Singer, K. D.; Weder, C. A Melt-processable Squaraine-Based Organic Glass for Nonlinear Optics. *J. Mater. Chem.* **2012**, *22*, 2848−2850.
(14) Ahn, H.-Y.; Yao, S.; Wang, X.; Belfield, K. D. Near-Infrared-Emitting Squaraine Dyes with High 2PA Cross-Sections for Multiphoton Fluorescence Imaging. *ACS Appl. Mater. Interfaces* **2012**, *4*, 2847−2854.
(15) Ramaiah, D.; Eckert, I.; Arun, K. T.; Weidenfeller, L.; Epe, B. Squaraine Dyes for Photodynamic Therapy: Mechanism of Cytotoxicity and DNA Damage Induced by Halogenated Squaraine Dyes Plus Light (>600 nm). *Photochem. Photobiol.* **2004**, *79*, 99−104.
(16) Ameri, T.; Heumuller, T.; Min, J.; Li, N.; Matt, G.; Scherf, U.; Brabec, C. J. IR Sensitization of an Indene-C60 Bisadduct (ICBA) in Ternary Organic Solar Cells. *Energy Environ. Sci.* **2013**, *6*, 1796−1801.
(17) Ameri, T.; Khoram, P.; Min, J.; Brabec, C. J. Organic Ternary Solar Cells: A Review. *Adv. Mater.* **2013**, *25*, 4245−4266.
(18) Cho, Y. J.; Lee, J. Y.; Chin, B. D.; Forrest, S. R. Polymer Bulk Heterojunction Photovoltaics Employing a Squaraine Donor Additive. *Org. Electron.* **2013**, *14*, 1081−1085.
(19) Kan, Z.; Colella, L.; Canesi, E. V.; Lerario, G.; Kumar, R. S. S.; Bonometti, V.; Mussini, P. R.; Cavallo, G.; Terraneo, G.; Pattanasattayavong, P.; Anthopoulos, T. D.; Bertarelli, C.; Keivanidis, P. E. Triple Bulk Heterojunctions as Means for Recovering the Microstructure of Photoactive Layers in Organic Solar Cell Devices. *Sol. Energy Mater. Sol. Cells* **2014**, *120* (Part A), 37−47.
(20) Yang, L.; Yan, L.; You, W. Organic Solar Cells beyond One Pair of Donor−Acceptor: Ternary Blends and More. *J. Phys. Chem. Lett.* **2013**, *4*, 1802−1810.
(21) Lunt, R. R.; Osedach, T. P.; Brown, P. R.; Rowehl, J. A.; Bulović, V. Practical Roadmap and Limits to Nanostructured Photovoltaics. *Adv. Mater.* **2011**, *23*, 5712−5727.
(22) Buhbut, S.; Itzhakov, S.; Tauber, E.; Shalom, M.; Hod, I.; Geiger, T.; Garini, Y.; Oron, D.; Zaban, A. Built-in Quantum Dot Antennas in Dye-Sensitized Solar Cells. *ACS Nano* **2010**, *4*, 1293−1298.
(23) Mor, G. K.; Basham, J.; Paulose, M.; Kim, S.; Varghese, O. K.; Vaish, A.; Yoriya, S.; Grimes, C. A. High-Efficiency Förster Resonance Energy Transfer in Solid-State Dye Sensitized Solar Cells. *Nano Lett.* **2010**, *10*, 2387−2394.
(24) Hardin, B. E.; Hoke, E. T.; Armstrong, P. B.; Yum, J.-H.; Comte, P.; Torres, T.; Fréchet, J. M. J.; Nazeeruddin, M. K.; Grätzel, M.; McGehee, M. D. Increased Light Harvesting in Dye-Sensitized Solar Cells with Energy Relay Dyes. *Nat. Photonics* **2009**, *3*, 406−411.
(25) Basham, J. I.; Mor, G. K.; Grimes, C. A. Förster Resonance Energy Transfer in Dye-Sensitized Solar Cells. *ACS Nano* **2010**, *4*, 1253−1258.
(26) Adhyaksa, G. W. P.; Lee, G. I.; Baek, S.-W.; Lee, J.-Y.; Kang, J. K., Broadband Energy Transfer to Sensitizing Dyes by Mobile Quantum Dot Mediators in Solar Cells. *Sci. Rep.* **2013**, *3*.
(27) Huang, J.-S.; Goh, T.; Li, X.; Sfeir, M. Y.; Bielinski, E. A.; Tomasulo, S.; Lee, M. L.; Hazari, N.; Taylor, A. D. Polymer Bulk Heterojunction Solar Cells Employing Förster Resonance Energy Transfer. *Nat. Photonics* **2013**, *7*, 479−485.
(28) Cnops, K.; Rand, B. P.; Cheyns, D.; Verreet, B.; Empl, M. A.; Heremans, P. 8.4% Efficient Fullerene-Free Organic Solar Cells Exploiting Long-Range Exciton Energy Transfer. *Nat. Commun.* **2014**, *5*, 3406−3412.
(29) Huang, J.-H.; Velusamy, M.; Ho, K.-C.; Lin, J.-T.; Chu, C.-W. A Ternary Cascade Structure Enhances the Efficiency of Polymer Solar Cells. *J. Mater. Chem.* **2010**, *20*, 2820−2825.
(30) Khlyabich, P. P.; Burkhart, B.; Thompson, B. C. Compositional Dependence of the Open-Circuit Voltage in Ternary Blend Bulk Heterojunction Solar Cells Based on Two Donor Polymers. *J. Am. Chem. Soc.* **2012**, *134*, 9074−9077.
(31) Lu, L.; Xu, T.; Chen, W.; Landry, E. S.; Yu, L. Ternary Blend Polymer Solar Cells with Enhanced Power Conversion Efficiency. *Nat. Photonics* **2014**, *8*, 716−722.
(32) Zimmerman, J. D.; Xiao, X.; Renshaw, C. K.; Wang, S.; Diev, V. V.; Thompson, M. E.; Forrest, S. R. Independent Control of Bulk and Interfacial Morphologies of Small Molecular Weight Organic Heterojunction Solar Cells. *Nano Lett.* **2012**, *12*, 4366−4371.
(33) Zimmerman, J. D.; Lassiter, B. E.; Xiao, X.; Sun, K.; Dolocan, A.; Gearba, R.; Vanden Bout, D. A.; Stevenson, K. J.; Wickramasinghe, P.; Thompson, M. E.; Forrest, S. R. Control of Interface Order by Inverse Quasi-Epitaxial Growth of Squaraine/Fullerene Thin Film Photovoltaics. *ACS Nano* **2013**, *7*, 9268−9275.
(34) Wei, G.; Xiao, X.; Wang, S.; Zimmerman, J. D.; Sun, K.; Diev, V. V.; Thompson, M. E.; Forrest, S. R. Arylamine-Based Squaraine Donors for Use in Organic Solar Cells. *Nano Lett.* **2011**, *11*, 4261−4264.
(35) Chen, Y.-H.; Lin, L.-Y.; Lu, C.-W.; Lin, F.; Huang, Z.-Y.; Lin, H.-W.; Wang, P.-H.; Liu, Y.-H.; Wong, K.-T.; Wen, J.; Miller, D. J.; Darling, S. B. Vacuum-Deposited Small-Molecule Organic Solar Cells with High Power Conversion Efficiencies by Judicious Molecular Design and Device Optimization. *J. Am. Chem. Soc.* **2012**, *134*, 13616−13623.
(36) Hu, L.; Yan, Z.; Xu, H. Advances in Synthesis and Application of Near-Infrared Absorbing Squaraine Dyes. *RSC Adv.* **2013**, *3*, 7667−7676.
(37) Tian, M.; Furuki, M.; Iwasa, I.; Sato, Y.; Pu, L. S.; Tatsuura, S. Search for Squaraine Derivatives That Can Be Sublimed without Thermal Decomposition. *J. Phys. Chem. B* **2002**, *106*, 4370−4376.
(38) Wang, S.; Hall, L.; Diev, V. V.; Haiges, R.; Wei, G.; Xiao, X.; Djurovich, P. I.; Forrest, S. R.; Thompson, M. E. *N*,*N*-Diarylanilinosquaraines and Their Application to Organic Photovoltaics. *Chem. Mater.* **2011**, *23*, 4789−4798.
(39) Odom, S. A.; Webster, S.; Padilha, L. A.; Peceli, D.; Hu, H.; Nootz, G.; Chung, S.-J.; Ohira, S.; Matichak, J. D.; Przhonska, O. V.; Kachkovski, A. D.; Barlow, S.; Brédas, J.-L.; Anderson, H. L.; Hagan, D. J.; Van Stryland, E. W.; Marder, S. R. Synthesis and Two-Photon Spectrum of a Bis(porphyrin)-Substituted Squaraine. *J. Am. Chem. Soc.* **2009**, *131*, 7510−7511.
(40) Feron, K.; Belcher, W.; Fell, C.; Dastoor, P. Organic Solar Cells: Understanding the Role of Förster Resonance Energy Transfer. *Int. J. Mol. Sci.* **2012**, *13*, 17019−17047.
(41) Wei, G.; Wang, S.; Renshaw, K.; Thompson, M. E.; Forrest, S. R. Solution-Processed Squaraine Bulk Heterojunction Photovoltaic Cells. *ACS Nano* **2010**, *4*, 1927−1934.
(42) Liang, Z.; Zhang, Q.; Wiranwetchayan, O.; Xi, J.; Yang, Z.; Park, K.; Li, C.; Cao, G. Effects of the Morphology of a ZnO Buffer Layer on the Photovoltaic Performance of Inverted Polymer Solar Cells. *Adv. Funct. Mater.* **2012**, *22*, 2194−2201.
(43) Xiao, X.; Wei, G.; Wang, S.; Zimmerman, J. D.; Renshaw, C. K.; Thompson, M. E.; Forrest, S. R. Small-Molecule Photovoltaics Based on Functionalized Squaraine Donor Blends. *Adv. Mater.* **2012**, *24*, 1956−1960.
(44) Street, R. A.; Davies, D.; Khlyabich, P. P.; Burkhart, B.; Thompson, B. C. Origin of the Tunable Open-Circuit Voltage in

DOI: 10.1021/ph500282z
ACS Photonics 2015, 2, 86−95

Ternary Blend Bulk Heterojunction Organic Solar Cells. *J. Am. Chem. Soc.* **2013**, *135*, 986−989.
(45) Groves, C. Suppression of Geminate Charge Recombination in Organic Photovoltaic Devices with a Cascaded Energy Hterojunction. *Energy Environ. Sci.* **2013**, *6*, 1546−1551.
(46) Giebink, N. C.; Wiederrecht, G. P.; Wasielewski, M. R.; Forrest, S. R. Ideal Diode Equation for Organic Heterojunctions. I. Derivation and Application. *Phys. Rev. B* **2010**, *82*, 155305.
(47) Giebink, N. C.; Lassiter, B. E.; Wiederrecht, G. P.; Wasielewski, M. R.; Forrest, S. R. Ideal Diode Equation for Organic Heterojunctions. II. The Role of Polaron Pair Recombination. *Phys. Rev. B* **2010**, *82*, 155306.
(48) Kang, H.; Kim, K.-H.; Kang, T. E.; Cho, C.-H.; Park, S.; Yoon, S. C.; Kim, B. J. Effect of Fullerene Tris-Adducts on the Photovoltaic Performance of P3HT:Fullerene Ternary Blends. *ACS Appl. Mater. Interfaces* **2013**, *5*, 4401−4408.
(49) Qi, B.; Wang, J. Fill Factor in Organic Solar Cells. *Phys. Chem. Chem. Phys.* **2013**, *15*, 8972−8982.
(50) Wei, G.; Xiao, X.; Wang, S.; Sun, K.; Bergemann, K. J.; Thompson, M. E.; Forrest, S. R. Functionalized Squaraine Donors for Nanocrystalline Organic Photovoltaics. *ACS Nano* **2011**, *6*, 972−978.
(51) Spencer, S.; Cody, J.; Misture, S.; Cona, B.; Heaphy, P.; Rumbles, G.; Andersen, J.; Collison, C. Critical Electron Transfer Rates for Exciton Dissociation Governed by Extent of Crystallinity in Small Molecule Organic Photovoltaics. *J. Phys. Chem. C* **2014**, *118*, 14840−14847.
(52) Sun, Y.; Seo, J. H.; Takacs, C. J.; Seifter, J.; Heeger, A. J. Inverted Polymer Solar Cells Integrated with a Low-Temperature-Annealed Sol-Gel-Derived ZnO Film as an Electron Transport Layer. *Adv. Mater.* **2011**, *23*, 1679−1683.
(53) Huang, J.-S.; Chou, C.-Y.; Lin, C.-F. Efficient and Air-Stable Polymer Photovoltaic Devices With WO3−V2O5 Mixed Oxides as Anodic Modification. *IEEE Electron Dev. Lett.* **2010**, *31*, 332−334.
(54) Kandada, A. R. S.; Grancini, G.; Petrozza, A.; Perissinotto, S.; Fazzi, D.; Raavi, S. S. K.; Lanzani, G., Ultrafast Energy Transfer in Ultrathin Organic Donor/Acceptor Blend. *Sci. Rep.* **2013**, *3*.
(55) Hardin, B. E.; Yum, J.-H.; Hoke, E. T.; Jun, Y. C.; Péchy, P.; Torres, T. s.; Brongersma, M. L.; Nazeeruddin, M. K.; Grätzel, M.; McGehee, M. D. High Excitation Transfer Efficiency from Energy Relay Dyes in Dye-Sensitized Solar Cells. *Nano Lett.* **2010**, *10*, 3077−3083.
(56) Snellenburg, J. J.; Laptenok, S.; Seger, R.; Mullen, K. M.; Stokkum, I. H. M. v. Glotaran: A Java-Based Graphical User Interface for the R Package TIMP. *J. Stat. Softw.* **2012**, *49*, 1−22.
(57) Yang, L.; Zhou, H.; Price, S. C.; You, W. Parallel-Like Bulk Heterojunction Polymer Solar Cells. *J. Am. Chem. Soc.* **2012**, *134*, 5432−5435.
(58) He, Z.; Zhong, C.; Su, S.; Xu, M.; Wu, H.; Cao, Y. Enhanced Power-Conversion Efficiency in Polymer Solar Cells Using an Inverted Device Structure. *Nat. Photonics* **2012**, *6*, 593−597.
(59) Xiao, X.; Bergemann, K. J.; Zimmerman, J. D.; Lee, K.; Forrest, S. R. Small-Molecule Planar-Mixed Heterojunction Photovoltaic Cells with Fullerene-Based Electron Filtering Buffers. *Adv. Energy Mater.* **2013**, *4*, 1301557.

DOI: 10.1021/ph500282z
ACS Photonics 2015, 2, 86−95